Aalborg Universitet

MIMO Transmission Using a Single RF Source: Theory and Antenna Design

Alrabadi, Osama Nafeth Saleem; Perruisseau-Carrier, Julien; Kalis, Antonis

MIMO Transmission Using a Single RF Source: Theory and Antenna Design

Osama N. Alrabadi, Julien Perruisseau-Carrier and Antonis Kalis
Members, IEEE

Abstract— An approach for transmitting multiple signals using a single switched parasitic antenna (SPA) has been recently reported. The idea there is to map the signals to be transmitted onto a set of basis functions that serve as 'virtual antennas' in the beamspace (i.e. wavevector) domain. In this work, we generalize the derivation of the antenna pattern basis functions regarding a 3-element SPA of arbitrary radiating elements, within a symmetric array topology, for multiplexing signals in the wavevector domain (using different beampatterns) rather than in the hardware antenna domain with multiple feeding ports. A fully operational antenna system example is modeled, optimized regarding its return loss and the power imbalance between the basis functions, and finally realized. The measurements of the SPA show good agreement with the simulated target values, revealing an accurate design approach to be adopted as a fast SPA prototyping methodology. The SPA has been successfully employed for multiplexing two BPSK datastreams over-the-air, thus paving the way for practically compact and highly efficient MIMO transceiver designs.

Index Terms— MIMO, Switched Parasitic Antenna, Basis functions, Reconfigurable Antenna.

I. INTRODUCTION

MULTI-INPUT MULTI-OUTPUT (MIMO) communication has gained lots of attention over the last decade as it enhances the spectral efficiency by exploiting the precious spatial resource dimension [1] [2]. Since the emergence of this technology, the classical approach has been assuming a transmitter with a number of transmit RF chains in order to independently map a set of signals onto a corresponding set of antennas. The receiver on the other hand performs some complex signal processing so as to decode the linear mixture of the signals and extract the useful data. However, having multiple RF chains at the user mobile terminal is rather costly. For example, the LTE - Release 8 standard supports a single antenna for the uplink transmission and two antennas for the downlink reception [3] [4]. The asymmetry in the number of antennas is mainly intended for avoiding the costly power amplifiers in the transmit RF chains. Although antenna selection is a terminal option, it requires instantaneous channel state information from the receiver back to the transmitter,

which is a burden on the wireless communication system. Consequently, classical MIMO transmission especially in uplink scenarios may not be supported due to the practical limitations of the portable RF units.

To overcome these challenges, the authors in [5] describe how a half rate space-time (ST) code is transmitted with a single radio. In fact, a simple time-switched ST code [6] will outperform the approach in [5] regarding both performance and complexity. In [7], the authors propose an antenna system of two RF sources and four antenna elements. The proposed antenna system is capable of changing its polarization state (at the modulation rate), and thus transmitting the 4×4 Jafarkhani code. However, having two transmit RF chains may still be costly for low-end terminals.

On the other hand, the authors in [8] proposed a MIMO-like system using a switched parasitic antenna (SPA) with a single RF source. The SPA was shown to have a throughput potential comparable to that of conventional MIMO systems by switching the SPA far-field at the modulation rate, however no specific multiplexing techniques were proposed. In fact, parasitic antenna systems have been proposed over the past as a promising solution for addressing the problems associated with the difficulty of integrating multiple RF chains in compact portable units [9]. Such antenna systems comprise a single RF branch and multiple antenna elements loaded by variable reactive impedances. By controlling the reactance via a DC control, basic antenna properties, like the beampattern, can be reconfigured. Parasitic antennas have been widely used for providing receive angular (or pattern) diversity (examples are given in [10] [11]) and have recently been proposed for analogue beam and null steering [12].

The use of a compact-sized SPA for emulating open-loop MIMO transmission has been first proposed in the work of Kalis *et al* in [13] followed by work of Alrabadi *et al* [14]. The idea of using an SPA as a MIMO terminal is to drive the central active antenna with a high frequency RF signal modulated by the first datastream, while simultaneously driving a set of parasitic elements (PE) strongly coupled to the active one with a baseband (low frequency) control signal as shown in Fig. 1. The baseband control signal has information about the other datastreams to be transmitted over the air. By this way, it has been shown that the input datastreams are mapped onto an orthogonal set of basis functions in the wavevector domain via a single radio and compact array dimensions.

In this paper we focus on BPSK signaling format (the extension to all PSK is straightforward by following the approach in [14]) where we first *generalize* the derivation

Osama N. Alrabadi is with the Antennas, Propagation and Radio Networking (APNet) group, Department of Electronic Systems, Aalborg University, DK-9220 Aalborg, Denmark. (e-mail: ona@es.aau.dk).

Julien Perruisseau-Carrier is with the group for Adaptive MicroNano Wave Systems, LEMA/Nanolab, Ecole Polytechnique Fdrale de Lausanne (EPFL), Lausanne CH-1015, Switzerland. email: (julien.perruisseau-carrier@epfl.ch).

Antonis Kalis is with the Broadband Wireless and Sensor Networks (BWiSE) Group, Athens Information Technology (AIT), GR-19002, Athens, Greece. email: (akal@ait.edu.gr).

of the bases from mirror image pattern pairs (MIPPs) i.e. when one beampattern is a mirrored version of the other, regardless of how the MIPPs are expressed. We therefore extend previous findings by decoupling the wavevector domain [15] from the antenna domain and thus enabling MIMO functionality through any antenna system capable of creating MIPPs. At the receiver side, we prove that the receive antenna response to a beampattern that is a linear mixture of basis functions, is nothing more than the linear combination of the receive antenna responses to the different basis functions. By this way, the receiver decodes the transmitted data symbols by estimating the basis responses using classical training techniques.

A practical antenna system example of printed dipoles is proposed, modeled, optimized regarding the average rate of transmission, finally designed and demonstrated. The measured return loss and radiation patterns are in good agreement with the target parameters, revealing a fast and accurate designing methodology.

Throughout the paper a bold small letter designates a vector and a bold big letter designates a matrix. The operators $()^*, ()^T, ()^H$ designate complex conjugate, transpose and complex conjugate transpose (Hermitian) operators, respectively. The notation $\mathbf{I}_N$ indicates an identity matrix of size $N \times N$. The operator $\text{diag}(\mathbf{v})$ returns a square matrix with the elements of the vector $\mathbf{v}$ laid across the main diagonal of the matrix. Moreover, we consider a classical uniform three-dimensional angular power spectrum seen by the transmitter (the mobile terminal), which is approximately the case when the mobile unit is surrounded by many scatterers.

The rest of the paper is organized as follows: in Section II we describe a technique for transmitting two BPSK signals simultaneously via a single RF frontend. Section III expresses the basis functions of a 3-element SPA based on full-wave electromagnetic modeling, and optimizes the SPA for BPSK signaling regarding the average rate of transmission. Section IV describes an SPA example of printed dipoles and explains its design implementation. Section V shows both simulation and measurement results and finally Section VI concludes the paper.

II. MIMO Transmission with a Single RF Source

In this section we first prove the existence of an orthogonal basis whenever a MIPP can be formed. Based on this, a technique for transmitting two BPSK signals using arbitrary single radio based antenna system capable of forming a MIPP is described.

A. Orthogonal Bases Using a MIPP

The correlation between two arbitrary beampatterns $\mathcal{G}_1(\vartheta, \varphi)$ and $\mathcal{G}_2(\vartheta, \varphi)$ is given by

$$\varrho_{12} = \frac{1}{\sqrt{P_1 P_2}} \int_\varphi \int_\vartheta \mathcal{G}_1(\vartheta, \varphi) \, \mathcal{G}_2^*(\vartheta, \varphi) \sin(\vartheta) \cdot d\vartheta d\varphi \quad (1)$$

where

$$P_1 = \frac{1}{4\pi} \int_\varphi \int_\vartheta |\mathcal{G}_1(\vartheta, \varphi)|^2 \sin(\vartheta) \cdot d\vartheta d\varphi,$$

$$P_2 = \frac{1}{4\pi} \int_\varphi \int_\vartheta |\mathcal{G}_2(\vartheta, \varphi)|^2 \sin(\vartheta) \cdot d\vartheta d\varphi, \quad (2)$$

are the spatial integration of the power beampatterns of $\mathcal{G}_1(\vartheta, \varphi)$ and $\mathcal{G}_2(\vartheta, \varphi)$ over the space, respectively. Whenever $P_1 = P_2$, the two beampatterns are called 'balanced'.

Lemma.1: For a MIPP $\mathcal{G}_1(\vartheta, \varphi)$ and $\mathcal{G}_2(\vartheta, \varphi)$, the set of the angular functions defined as

$$\mathcal{B}_\Sigma(\vartheta, \varphi) := \frac{1}{\sqrt{2}} \big(\mathcal{G}_2(\vartheta, \varphi) + \mathcal{G}_1(\vartheta, \varphi)\big),$$

$$\mathcal{B}_\Delta(\vartheta, \varphi) := \frac{1}{\sqrt{2}} \big(\mathcal{G}_2(\vartheta, \varphi) - \mathcal{G}_1(\vartheta, \varphi)\big), \quad (3)$$

form an orthogonal basis.

Proof: For two beampatterns that form a MIPP, we have $P_1 = P_2$ since one beampattern is just a mirrored version of the other. Moreover, the correlation between the two beams is *real* (see the proof at Appendix), and thus $\varrho_{12} = \varrho_{12}^*$. Based on these observations, the proof is straightforward and is given in (4) on top of page 3.

∎

Corollary.1: A balanced basis is obtained by designing the two beampatterns $\mathcal{G}_1(\vartheta, \varphi)$ and $\mathcal{G}_2(\vartheta, \varphi)$ described in **Lemma.1** to be orthogonal to each other i.e. if $\mathcal{G}_1(\vartheta, \varphi)$ and $\mathcal{G}_2(\vartheta, \varphi)$ are orthonormal, $\mathcal{B}_\Sigma(\vartheta, \varphi)$ and $\mathcal{B}_\Delta(\vartheta, \varphi)$ are orthonormal too[1].

Proof: Let $\mathcal{G}_1(\vartheta, \varphi) \perp \mathcal{G}_2(\vartheta, \varphi)$, the proof is straightforward as shown in (6) on top of page 3. In (6), P_Σ and P_Δ are the spatial integration of the power beampatterns of $\mathcal{B}_\Sigma(\vartheta, \varphi)$ and $\mathcal{B}_\Delta(\vartheta, \varphi)$, over the space, given respectively by

$$P_\Sigma = \frac{1}{4\pi} \int_\varphi \int_\vartheta |\mathcal{B}_\Sigma(\vartheta, \varphi)|^2 \sin(\vartheta) \cdot d\vartheta d\varphi,$$

$$P_\Delta = \frac{1}{4\pi} \int_\varphi \int_\vartheta |\mathcal{B}_\Delta(\vartheta, \varphi)|^2 \sin(\vartheta) \cdot d\vartheta d\varphi. \quad (5)$$

∎

B. Transmission Technique Description

In this part we show that an arbitrary antenna system having a single RF input but has the capability of creating a MIPP will be capable of transmitting two BPSK signals s_1 and s_2, simultaneously. The two BPSK signals are mapped onto an orthogonal set of basis functions, thus independent fading between the two signals is almost always guaranteed regardless of the transceiver compactness. Let the sole RF port be fed by the signal s_1, the antenna beampattern in the far-field becomes either

---

[1]The reason we acquire an orthonormal basis $\mathcal{B}_\Sigma(\vartheta, \varphi)$ and $\mathcal{B}_\Delta(\vartheta, \varphi)$ from a MIPP, is that the MIPP by itself represents a linear combination (desired multiplexing relation) of the basis onto which the signals are mapped. The diversity action of the system directly depends on the transmit covariance of the basis (proportional to the identity matrix when the basis is orthonormal).

$$\begin{aligned}
\varrho_{\Sigma\Delta} &= \frac{1}{4\pi\sqrt{P_\Sigma P_\Delta}} \int_\varphi \int_\vartheta \mathcal{B}_\Sigma(\vartheta,\varphi)\,\mathcal{B}_\Delta^*(\vartheta,\varphi)\sin(\vartheta)\cdot d\vartheta d\varphi \\
&= \frac{1}{8\pi\sqrt{P_\Sigma P_\Delta}} \int_\varphi \int_\vartheta \left(\mathcal{G}_2(\vartheta,\varphi)+\mathcal{G}_1(\vartheta,\varphi)\right)\left(\mathcal{G}_2^*(\vartheta,\varphi)-\mathcal{G}_1^*(\vartheta,\varphi)\right)\sin(\vartheta)\cdot d\vartheta d\varphi \\
&= \frac{1}{2\sqrt{P_\Sigma P_\Delta}}\left(P_2 - \sqrt{P_1 P_2}\varrho_{12}^* + \sqrt{P_1 P_2}\varrho_{12} - P_1\right) \\
&= \frac{1}{2\sqrt{P_\Sigma P_\Delta}}\left(P_1 - P_1\varrho_{12} + P_1\varrho_{12} - P_1\right) \\
&= 0
\end{aligned} \tag{4}$$

$$\begin{aligned}
0 &= \frac{1}{4\pi\sqrt{P_1 P_2}} \int_\varphi \int_\vartheta \mathcal{G}_1(\vartheta,\varphi)\,\mathcal{G}_2^*(\vartheta,\varphi)\sin(\vartheta)\cdot d\vartheta d\varphi \\
0 &= \frac{1}{8\pi\sqrt{P_1 P_2}} \int_\varphi \int_\vartheta \left(\mathcal{B}_\Sigma(\vartheta,\varphi)-\mathcal{B}_\Delta(\vartheta,\varphi)\right)\left(\mathcal{B}_\Sigma^*(\vartheta,\varphi)+\mathcal{B}_\Delta^*(\vartheta,\varphi)\right)\sin(\vartheta)\cdot d\vartheta d\varphi \\
0 &= \frac{1}{2\sqrt{P_1 P_2}}\left(P_\Sigma + \varrho_{\Sigma\Delta}\sqrt{P_\Sigma P_\Delta} - \varrho_{\Sigma\Delta}^*\sqrt{P_\Sigma P_\Delta} - P_\Delta\right) \\
0 &= \frac{1}{2\sqrt{P_1 P_2}}\left(P_\Sigma - P_\Delta\right) \\
\Rightarrow\quad P_\Sigma &= P_\Delta
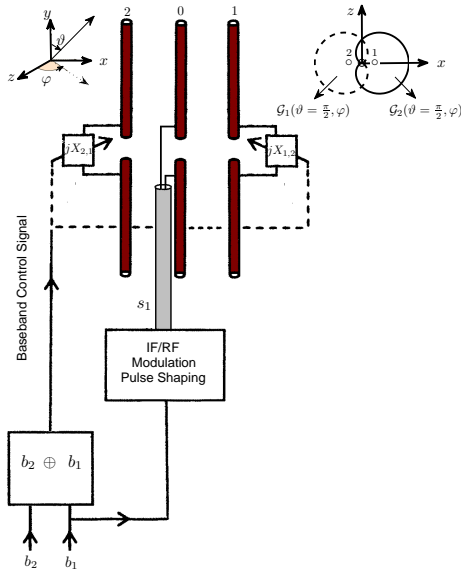\end{aligned} \tag{6}$$

Fig. 1. Schematic diagram of the proposed technique where the first bitstream is modulated, up converted and fed into the central active element whereas the second bitstream is XORed with the first one. The output control signal is used for swapping the loads of the PE.

where S is the antenna system state such that $S := 1$ is *State 1* within which the antenna system transmits over $\mathcal{G}_1(\vartheta,\varphi)$ and $S := 2$ is *State 2* within which the antenna system transmits over $\mathcal{G}_2(\vartheta,\varphi)$. From (7b) it is obvious how the two BPSK signals: s_1 which is modulated in the baseband, up-converted and fed into the input RF port and $s_2 = (-1)^S s_1$ which is spatially modulated on the antenna far-field by controlling the antenna state S, are mapped onto the space of $\mathcal{B}_\Sigma(\vartheta,\varphi)$ and $\mathcal{B}_\Delta(\vartheta,\varphi)$, respectively. In general, for any PSK modulation of order N, s_2 is a set of N complex numbers evenly distributed over the unit circle, as discussed in Section IV of [12]. Table I shows the state S required for transmitting s_2 according to the value of s_1 where $[b_1\ b_2]^T$ is input vector of bits modulated into $[s_1\ s_2]^T$. Fig. 1 shows a schematic diagram of the proposed technique, where the XORing of the two bitstreams gives the required S i.e. $S = b_1 \oplus b_2$ giving 0 and 1 which correspond to $S := 1$ and $S := 2$, respectively.

TABLE I
TWO BPSK SIGNALS COMBINATIONS

$[b_1\ b_2]^T$	$[s_1\ s_2]^T$	S
$[\ 1\quad 1\ ]^T$	$[\ 1\quad 1\ ]^T$	2
$[\ 1\quad 0\ ]^T$	$[\ 1\ -1\ ]^T$	1
$[\ 0\quad 1\ ]^T$	$[-1\quad 1\ ]^T$	1
$[\ 0\quad 0\ ]^T$	$[-1\ -1\ ]^T$	2

C. System Training

The two BPSK signals that are transmitted in the beam-space domain and received using a classical uniform linear array of n_R antenna elements (n_R-element ULA), can be

$$\begin{aligned}
&\text{State 1} \\
\mathcal{G}_T(\vartheta,\varphi) &= \mathcal{G}_1(\vartheta,\varphi)\,s_1 \\
&= \frac{s_1}{\sqrt{2}}\left[\mathcal{B}_\Sigma(\vartheta,\varphi)-\mathcal{B}_\Delta(\vartheta,\varphi)\right] \\
&\text{or State 2} \\
\mathcal{G}_T(\vartheta,\varphi) &= \mathcal{G}_2(\vartheta,\varphi)\,s_1 \\
&= \frac{s_1}{\sqrt{2}}\left[\mathcal{B}_\Sigma(\vartheta,\varphi)+\mathcal{B}_\Delta(\vartheta,\varphi)\right] \\
&\text{or generally as} \\
\mathcal{G}_T(\vartheta,\varphi) &= \frac{s_1}{\sqrt{2}}\left[\mathcal{B}_\Sigma(\vartheta,\varphi)+(-1)^S\mathcal{B}_\Delta(\vartheta,\varphi)\right] \quad (7a) \\
&= \frac{1}{\sqrt{2}}\left[s_1\mathcal{B}_\Sigma(\vartheta,\varphi)+s_2\mathcal{B}_\Delta(\vartheta,\varphi)\right] \quad (7b)
\end{aligned}$$

decoded by first estimating the receive antenna responses to the proposed basis.

Proposition.1: A beampattern comprising a linear mixture of basis functions (at the transmitter side) triggers a linear combination of the individual channel responses to the different basis functions (at the receiver side).

Proof: This directly stems from the principle of superposition in linear systems. To have a deeper insight, we first define 2×1 column vectors $\mathcal{G}_{1,T}(\vartheta, \varphi)$, $\mathcal{G}_{2,T}(\vartheta, \varphi)$, $\mathcal{B}_{\Sigma,T}(\vartheta, \varphi)$ and $\mathcal{B}_{\Delta,T}(\vartheta, \varphi)$, where the first and the second elements of every column vector represent the $\hat{\vartheta}$ and $\hat{\varphi}$ polarizations of the corresponding pattern, respectively. We also define $\mathcal{G}_{k,R}(\vartheta, \varphi)$ as the vector of the polarization components of the kth receiver antenna pattern $\mathcal{G}_{k,R}(\vartheta, \varphi)$. As in [16], we assume that the propagation channel between the transmitter and the receiver consists of a set of L plane waves, with the lth wave characterized by a complex voltage gain β_l, angle of departure $(\vartheta_{l,T}, \varphi_{l,T})$, and angle of arrival $(\vartheta_{l,R}, \varphi_{l,R})$. We also assume that each plane wave undergoes a polarization transformation due to scattering that can be expressed as the unitary matrix

$$\mathbf{O}_l = \left[\begin{array}{cc} o_{l,\vartheta\vartheta} & o_{l,\vartheta\varphi} \\ o_{l,\varphi\vartheta} & o_{l,\varphi\varphi} \end{array} \right]. \tag{8}$$

The response of the kth receive antenna ($1 \leq k \leq n_R$) when illuminated by the beampattern $\mathcal{G}_1(\vartheta, \varphi)$ is the complex channel gain representing the ratio of the received voltage signal to the transmitted voltage signal, and may be written as shown in (9), where $C_{k,1}$ is a constant that depends on the receiver and the transmitter active gains and impedances [17], $h_{k,\Sigma}$ and $h_{k,\Delta}$ are the responses of the kth receive antenna to $\mathcal{B}_{\Sigma}(\vartheta, \varphi)$ and $\mathcal{B}_{\Delta}(\vartheta, \varphi)$, respectively. By applying the same analysis, the response of the kth receive antenna when illuminated by $\mathcal{G}_2(\vartheta, \varphi)$ becomes $h_{k2} = \frac{1}{\sqrt{2}}(h_{k,\Sigma} + h_{k,\Delta})$. ∎

Based on this, the receiver can decode the two BPSK signals by estimating the channel responses of the basis as

$$h_{k,\Sigma} = \frac{1}{\sqrt{2}}(h_{k,1} + h_{k,2}), \tag{10a}$$

$$h_{k,\Delta} = \frac{1}{\sqrt{2}}(h_{k,1} - h_{k,2}). \tag{10b}$$

By constructing the matrix of the receive antennas' responses, the receiver can zero-force the received signal by inverting the channel matrix (or using any other reception techniques) for decoding s_1 and s_2.

III. ANTENNA MODEL AND OPTIMIZATION

In this paper we adopt the antenna topology proposed in [14], i.e. a symmetrical 3-element SPA, where the central element is the active one while the other two are passive. The two parasitic elements are loaded with pure imaginary loads $[jX_1 \ jX_2]$ as the real part of a complex load degrades the efficiency of the antenna system. Obviously the antenna system can create a MIPP around the E-plane (the yz plane in Fig. 1) by simply permuting the reactive loads

of the PE as $[jX_1 \ jX_2] \leftrightarrow [jX_2 \ jX_1]$, based on image theory. In other words, having the first beampattern $\mathcal{G}_1(\vartheta, \varphi)$ at $[jX_1 \ jX_2]$, the beampattern $\mathcal{G}_2(\vartheta, \varphi) = \mathcal{G}_1(\vartheta, -\varphi)$ is obtained at $[jX_2 \ jX_1]$. Consequently, by feeding the central active element with the first BPSK datastream and permuting the loads according to the second datastream, the two streams are simultaneously transmitted out of a single radio and mapped onto an orthogonal basis according to **Lemma.1**, irrespective of X_1 and X_2. Having the two loads X_1 and X_2 as a degree of freedom when considering BPSK signaling, we can optimize the loads according to a specific criterion as shown in Subsection III.C.

A. Generalized Derivation of Antenna Basis Functions

Although the beampattern of thin electrical dipoles (or monopoles) can be practically approximated as an array factor by the superposition of the retarded currents induced on the wire antenna elements such as in Eq. (6) in [14], this is not true when considering general[2] radiating elements e.g. flat or fractal dipoles, slot antennas etc. To overcome this problem, we implement full wave electromagnetic modeling based on the SPA scattering parameters (S-parameters) denoted by $\mathcal{S}_{ij}, \{i,j\} \in \{0,1,2\}$, as well as the 3D complex active port patterns[3] of the antenna elements 0, 1 and 2 shown in Fig. 1, denoted by $E_0(\vartheta, \varphi)$, $E_1(\vartheta, \varphi)$ and $E_2(\vartheta, \varphi)$, respectively. An expression of the electric far-field beampattern of a 3-element SPA based on the aforementioned quantities and the variable antenna loading has been derived in [19] using Mason's rule. From [19] and after correcting the equations to properly adhere to Masons Rule, the two basis functions obtained when swapping the imaginary loads of the two parasitic elements become

$$\mathcal{B}_{\Sigma}(\vartheta, \varphi) = \sqrt{2} E_0(\vartheta, \varphi)$$
$$+ \frac{1}{\sqrt{2}} \left(\mathcal{L}_1^1 + \mathcal{L}_1^2 \right) E_1(\vartheta, \varphi) + \left(\mathcal{L}_2^1 + \mathcal{L}_2^2 \right) E_2(\vartheta, \varphi)$$

$$\mathcal{B}_{\Delta}(\vartheta, \varphi) = \frac{1}{\sqrt{2}} \left(\mathcal{L}_1^1 - \mathcal{L}_1^2 \right) E_1(\vartheta, \varphi) + \left(\mathcal{L}_2^1 - \mathcal{L}_2^2 \right) E_2(\vartheta, \varphi)$$

$$\tag{11}$$

where

$$\mathcal{L}_1^1 = \frac{\Gamma_1 \mathcal{S}_{10}(1 - \Gamma_2 \mathcal{S}_{22}) + \Gamma_1 \Gamma_2 \mathcal{S}_{12} \mathcal{S}_{20}}{1 - \Gamma_1 \mathcal{S}_{11} - \Gamma_2 \mathcal{S}_{22} + \Gamma_1 \Gamma_2 \mathcal{S}_{11} \mathcal{S}_{22} - \Gamma_1 \Gamma_2 \mathcal{S}_{12} \mathcal{S}_{21}}$$

$$\mathcal{L}_1^2 = \frac{\Gamma_2 \mathcal{S}_{10}(1 - \Gamma_1 \mathcal{S}_{22}) + \Gamma_1 \Gamma_2 \mathcal{S}_{12} \mathcal{S}_{20}}{1 - \Gamma_2 \mathcal{S}_{11} - \Gamma_1 \mathcal{S}_{22} + \Gamma_1 \Gamma_2 \mathcal{S}_{11} \mathcal{S}_{22} - \Gamma_1 \Gamma_2 \mathcal{S}_{12} \mathcal{S}_{21}}$$

$$\mathcal{L}_2^1 = \frac{\Gamma_1 \mathcal{S}_{20}(1 - \Gamma_2 \mathcal{S}_{11}) + \Gamma_1 \Gamma_2 \mathcal{S}_{21} \mathcal{S}_{10}}{1 - \Gamma_1 \mathcal{S}_{11} - \Gamma_2 \mathcal{S}_{22} + \Gamma_1 \Gamma_2 \mathcal{S}_{11} \mathcal{S}_{22} - \Gamma_1 \Gamma_2 \mathcal{S}_{12} \mathcal{S}_{21}}$$

$$\mathcal{L}_2^2 = \frac{\Gamma_2 \mathcal{S}_{20}(1 - \Gamma_1 \mathcal{S}_{11}) + \Gamma_1 \Gamma_2 \mathcal{S}_{21} \mathcal{S}_{10}}{1 - \Gamma_2 \mathcal{S}_{11} - \Gamma_1 \mathcal{S}_{22} + \Gamma_1 \Gamma_2 \mathcal{S}_{11} \mathcal{S}_{22} - \Gamma_1 \Gamma_2 \mathcal{S}_{12} \mathcal{S}_{21}} \tag{12}$$

[2]Again we emphasize that the arbitrariness of the elements is limited to the center element being a self mirror image, and the outer two being respective mirror images of each other, both about a vertical plane that divides the left and right sides of the SPA structure

[3]The active port pattern is defined as the beampattern obtained when driving the corresponding port (whether being active or passive) with a unit excitation voltage signal while terminating the other ports with reference impedances [18].

$$h_{k1} = C_{k1} \sum_{l=1}^{L} \boldsymbol{\mathcal{G}}_{k,R} \left(\vartheta_{l,R}, \varphi_{l,R} \right) \beta_l \mathbf{O}_l \boldsymbol{\mathcal{G}}_{1,T} \left(\vartheta_{l,T}, \varphi_{l,T} \right)$$

$$= C_{k1} \sum_{l=1}^{L} \boldsymbol{\mathcal{G}}_{k,R} \left(\vartheta_{l,R}, \varphi_{l,R} \right) \beta_l \mathbf{O}_l \left(\boldsymbol{\mathcal{B}}_{\Sigma,T} \left(\vartheta_{l,T}, \varphi_{l,T} \right) - \boldsymbol{\mathcal{B}}_{\Delta,T} \left(\vartheta_{l,T}, \varphi_{l,T} \right) \right)$$

$$= C_{k1} \sum_{l=1}^{L} \boldsymbol{\mathcal{G}}_{k,R} \left(\vartheta_{l,R}, \varphi_{l,R} \right) \beta_l \mathbf{O}_l \boldsymbol{\mathcal{B}}_{\Sigma,T} \left(\vartheta_{l,T}, \varphi_{l,T} \right) - C_{k1} \sum_{l=1}^{L} \boldsymbol{\mathcal{G}}_{k,R} \left(\vartheta_{l,R}, \varphi_{l,R} \right) \beta_l \mathbf{O}_l \boldsymbol{\mathcal{B}}_{\Delta,T} \left(\vartheta_{l,T}, \varphi_{l,T} \right)$$

$$= \frac{1}{\sqrt{2}} \left(h_{k,\Sigma} - h_{k,\Delta} \right) \tag{9}$$

and $\mathcal{S}_{ij} \in \boldsymbol{\mathcal{S}}$ such that

$$\boldsymbol{\mathcal{S}} = \begin{bmatrix} \mathcal{S}_{00} & \mathcal{S}_{01} & \mathcal{S}_{02} \\ \mathcal{S}_{10} & \mathcal{S}_{11} & \mathcal{S}_{12} \\ \mathcal{S}_{20} & \mathcal{S}_{21} & \mathcal{S}_{22} \end{bmatrix}, \tag{13}$$

$$\Gamma_k = \left(jX_k + Z_0 \right)^{-1} \left(jX_k - Z_0 \right), \ k \in \{1, 2\}, \tag{14}$$

where we assumed $\Gamma_0 = 0$ by having the source impedance at the central driven port equal to the reference impedance $Z_0 = 50\,\Omega$. The basis coefficients in (12) are derived with respect to a general scattering matrix. Swapping the two reactive loads as $[\Gamma_1 \ \Gamma_2] \leftrightarrow [\Gamma_2 \ \Gamma_1]$, swaps the coefficients $\left(\mathcal{L}_k^1 - \mathcal{L}_k^2 \right) \leftrightarrow \left(\mathcal{L}_k^2 - \mathcal{L}_k^1 \right)$, $k \in \{1, 2\}$ in (11), thus phase-shifting $\mathcal{B}_\Delta \left(\vartheta, \varphi \right)$ by $180°$ without affecting $\mathcal{B}_\Sigma \left(\vartheta, \varphi \right)$. By this way, the $(-1)^S$ factor in (7a) is obtained. The two functions $\mathcal{B}_\Delta \left(\vartheta, \varphi \right)$ and $\mathcal{B}_\Sigma \left(\vartheta, \varphi \right)$ are the basis functions that are used to transmit two PSK signals of any modulation order [14].

B. Received Signal Model

Considering a narrowband, flat-fading, point-to-point communication link where the two BPSK symbols are transmitted in the beam-space domain over two basis functions (equivalent to two uncorrelated virtual antennas) and received using an n_R-element ULA of uncorrelated and uncoupled antenna elements. Assuming independent fading statistics at the transmitter and the receiver, the Kronecker product [20] can be assumed and thus the channel transfer function can be written as[4]

$$\mathbf{H}_{ch} = \mathbf{H}_w \mathbf{R}_T^{1/2}, \tag{15}$$

where the elements of the matrix $\mathbf{H}_w \in \mathbb{C}^{n_R \times 2}$ are independent and identically distributed (i.i.d.) complex Gaussian random variables with zero mean and unit variance. The correlation at the receiver side is ignored by the aforementioned assumptions regarding the receiving ULA. Defining the row vector $\boldsymbol{\mathcal{B}} \left(\vartheta, \varphi \right) = [\mathcal{B}_\Sigma \left(\vartheta, \varphi \right) \ \mathcal{B}_\Delta \left(\vartheta, \varphi \right)]$, the transmit

[4]In [21], the correlation based channel model accounts for the mutual coupling by explicitly incorporating the coupling matrices. However in (15), the mutual coupling is implicitly taken into consideration within the calculation of the basis functions in (11).

covariance matrix[5] $\mathbf{R}_T$ is obtained as

$$\mathbf{R}_T = \frac{1}{4\pi} \int_\varphi \int_\vartheta \boldsymbol{\mathcal{B}}^H \left(\vartheta, \varphi \right) \boldsymbol{\mathcal{B}} \left(\vartheta, \varphi \right) \sin \left(\vartheta \right) \cdot d\vartheta d\varphi,$$

$$= \begin{bmatrix} P_\Sigma & \varrho_{\Sigma\Delta} \sqrt{P_\Sigma P_\Delta} \\ \varrho_{\Sigma\Delta}^* \sqrt{P_\Sigma P_\Delta} & P_\Delta \end{bmatrix},$$

$$= \mathrm{diag} \left[P_\Sigma \ P_\Delta \right], \tag{16}$$

which is simply the power distribution across the basis functions since $\varrho_{\Sigma\Delta} = 0$ according to **Lemma.1**. Notice that $P_\Sigma + P_\Delta = P_1 + P_2 = 2P_1 = P_t$, which is easily obtained from (2) and the basis definition in (3), where P_t is the average transmit power. Defining the power imbalance ratio between the basis functions as $r = \frac{P_\Sigma}{P_\Delta}$, we can write $\mathbf{R}_T$ as $P_t \mathbf{Q}$ where $\mathbf{Q}$ is the normalized power distribution across the basis functions such that $\mathrm{trace}\{\mathbf{Q}\} = 1$. $\mathbf{Q}$ can be written as $\mathrm{diag}([q_1 \ q_2])$ such that $q_1 = r/(1 + r)$ and $q_2 = 1/(1 + r)$. From the above, the received signal model becomes

$$\begin{aligned} \mathbf{y} &= \sqrt{P_t} \mathbf{H}_w \mathbf{Q}^{1/2} \mathbf{s} + \mathbf{n} \\ &= \sqrt{P_i \Delta_T} \underbrace{\mathbf{H}_w \mathbf{Q}^{1/2}}_{\mathbf{H}} \mathbf{s} + \mathbf{n} \end{aligned} \tag{17}$$

where P_i is the power into the transmitter (input power) and $0 \leq \Delta_T \leq 1$ is the efficiency of the transmit antenna system being equal to $\Delta_T = 1 - |\Gamma|^2$, where Γ is the SPA return loss derived in [19]. Finally $\mathbf{s} = [s_1 \ s_2]^T$ is the vector of the modulated BPSK signals (see TABLE I), and $\mathbf{n}$ is a vector representing the white Gaussian noise, with zero mean and σ_n^2 variance.

C. Optimization Criterion

In this work, we define the optimal SPA loads as the ones that maximize the average rate of transmission. However, in MIMO communications, average rate computation often demands tackling calculations of expectations with respect to random matrices rather than random scalar variables. For this reason, we derive an upperbound on the average rate and deploy it as an optimization criterion. We assume open-loop operation where the channel is known to the receiver but unknown to the transmitter. The ergodic capacity of a MIMO

[5]Since the basis functions are imbalanced, the transmit covariance matrix rather than the transmit correlation matrix is considered.

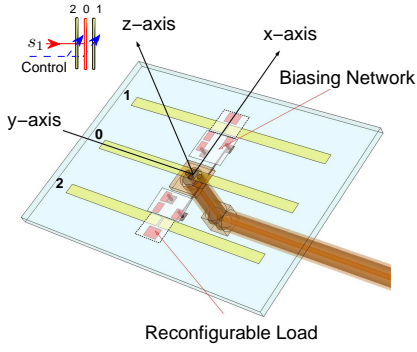Fig. 2. Schematic diagram of the SPA initially proposed in [24].

Fig. 3. An optimization contour map regarding the upperbound on $\Im_{av}$ with respect to X_1 and X_2.

random channel, denoted by $\Im_{av}$, is the ensemble average of the information rate over the distribution of the elements of the channel matrix $\mathbf{H} = \mathbf{H}_w \mathbf{Q}^{1/2} \in \mathbb{C}^{n_R \times 2}$. By using the $\log_2 \det(\cdot)$ formula [22], the upper bound that comes from the Jensen's inequality and the concavity of $\log_2 \det(\cdot)^6$, we get

$$\begin{aligned}
\Im_{av} &= \mathbb{E}_{\mathbf{H}} \left[\log_2 \det \left(\mathbf{I}_2 + \frac{P_i \Delta_T}{\sigma_n^2} \mathbf{H}^H \mathbf{H} \right) \right] \\
&\leq \log_2 \det \left(\mathbf{I}_2 + \frac{P_i \Delta_T}{\sigma_n^2} \mathbb{E}_{\mathbf{H}} \left[\mathbf{H}^H \mathbf{H} \right] \right) \\
&= \log_2 \det \left(\mathbf{I}_2 + \frac{P_i \Delta_T}{\sigma_n^2} \mathbf{Q} \right) \\
&= \log_2 \left(1 + \frac{P_i \Delta_T r}{\sigma_n^2 (1+r)^2} \right).
\end{aligned} \tag{18}$$

In (18), the average transmitted power is not divided by the number of the basis functions (the number of the virtual antennas), since the trace of $\mathbf{Q}$ is normalized to a unity rather than to the number of the basis functions (both forms are equivalent). The optimal loading is defined as the one that maximizes the average throughput upperbound in (18) i.e.

$$[X_1 \ X_2]_{opt} = \arg \max_{[X_1 \ X_2]} \left\{ \log_2 \left(1 + \frac{P_i \Delta_T r}{\sigma_n^2 (1+r)^2} \right) \right\}. \tag{19}$$

In (19), Δ_T is made part of the optimization criterion by constraining P_i rather than P_t as the SPA efficiency is a key design parameter when considering portable RF units with limited storage batteries.

IV. ANTENNA SYSTEM DESIGN

In this section we consider the 3-element SPA shown in Fig. 2, where the radiating elements are thin printed dipoles. The planar topology of the SPA makes it better fit in compactness-constrained mobile units as compared to the majority of the wire parasitic antennas already proposed in the literature. The current SPA was proposed earlier in [24], however in this paper we complete the work by describing the implementation and the measurements of the prototype.

[6]The $\log_2 \det(\cdot)$ is concave over positive semi-definite matrices [23]. Since $\mathbf{Q}$ is positive semi-definite, the term $\mathbf{I}_2 + \frac{P_i \Delta_T}{\sigma_n^2} \mathbf{Q}$ is positive semi-definite too, as it is a one-to-one mapping of $\mathbf{Q}$, thus preserving the positive definiteness.
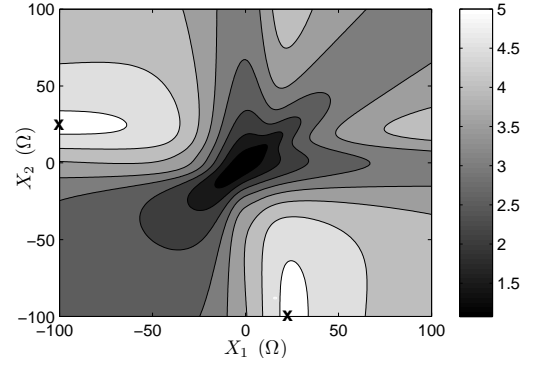
A. Design Parameters and Optimal Loading

The first design steps consist of making some initial choices on the antenna materials and the basic topology. We consider a 3-element SPA of flat dipoles as radiating elements as shown in Fig. 2, designed on an $h = 1.5$ mm thick substrate of relative permittivity $\varepsilon = 2.17$. The dipole lengths and spacing are 48.3 mm and 11 mm, respectively. The spacing is $\sim 0.1\lambda$ at the desired operational frequency of 2.6 GHz. The SPA was simulated using HFSS®, with ports at the locations of the variable loads. The resulting scattering matrix is given by

$$\boldsymbol{S} = \begin{bmatrix} -0.43 + \jmath 0.09 & 0.51 - \jmath 0.09 & 0.51 - \jmath 0.09 \\ 0.51 - \jmath 0.09 & -0.26 + \jmath 0.14 & 0.22 - \jmath 0.23 \\ 0.51 - \jmath 0.09 & 0.22 - \jmath 0.23 & -0.26 + \jmath 0.14 \end{bmatrix}, \tag{20}$$

where the matrix is symmetric by the reciprocity theorem i.e. by the usual assumption of employing antennas with electrically reciprocal materials, thus $\boldsymbol{S}_{ij} = \boldsymbol{S}_{ji}$. Moreover, the symmetric topology of the SPA shown in Fig. 1 ensures that $\boldsymbol{S}_{02} = \boldsymbol{S}_{01}$ and $\boldsymbol{S}_{22} = \boldsymbol{S}_{11}$. The antenna system is lossy as $\boldsymbol{S}^H \boldsymbol{S} \neq \mathbf{I}_3$ when compared to the lossless 4-port network (expressed by $\boldsymbol{S}_{EQ}$) in [19] as $\boldsymbol{S}_{EQ}^H \boldsymbol{S}_{EQ} = \mathbf{I}_4$ by the energy conservation principle when including the radiated beams in the network structure. Further, the diagonal elements of $\boldsymbol{S}$ are non-vanishing as we aim at diminishing the return loss of the central active element rather than $\boldsymbol{S}_{ii}$. The resulting 3-port S-parameters and the complex 3D active port patterns were exported to MATLAB®, where a computer routine scans the realizable range of the reactance space searching for $[X_1 \ X_2]_{opt}$ given by (19). Fig. 3 shows an optimization contour plot of $\Im_{av}(X_1, X_2)$ at a transmit signal to noise ratio[7] (SNR) $P_i / \sigma_n^2 = 10$ dB. The figure shows that $\Im_{av}$ is maximized at $[X_1 \ X_2]_{opt} = [-100 \ +27] \ \Omega$. At such loading, the upperbound on $\Im_{av}$ is 5 b/s/Hz, the power imbalance between the two basis functions is 0.56 dB, and the SPA

[7]In fact, the transmit SNR P_t / σ_n^2 is commonly used in the literature when evaluating the system performance. However, as the SPA loading will affect the transmit SNR through the matching efficiency, it seems more reasonable to use P_i / σ_n^2 which is simply the transmit SNR before the mismatch effect represented by Δ_T. On the other hand, the way of calculating the receive SNR is different and is shown later in Eq. (20).
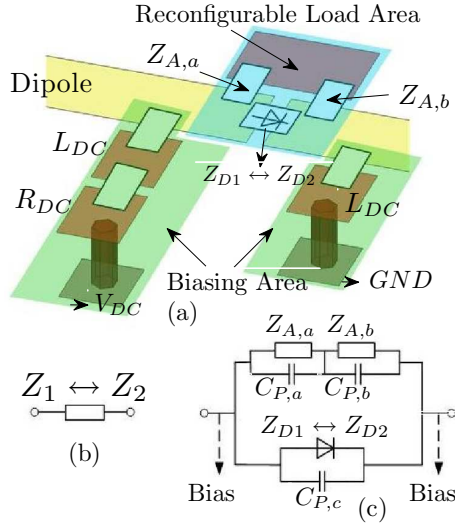
Fig. 4. Reconfigurable dipole load impedance: (a) Layout and elements view, including biasing network, (b) target two-state variable impedance and (c) detailed implementation circuit, including layout parasitic capacitances.

efficiency is 97%.

B. Reconfigurable Impedance Implementation

The design of the variable load, explained in more detail in the earlier partial work of [24], consists of the following steps: First, an adequate layout for the reconfigurable load area, to be controlled using a PIN diode, is selected ('Reconfigurable Load Area' in Fig. 4a). The parasitic capacitance ($C_{P,a}$, $C_{P,b}$, and $C_{P,c}$) between the different pads are extracted from full-wave simulations. Here the inductive effect in the pads can be neglected in the design. Subsequently, the surface-mounted elements to implement $Z_{A,a}$ and $Z_{A,b}$ are deduced from the circuit of Fig. 4 so that the overall impedance in each state Z_1 and Z_2 (see Fig. 4b) match the target values deduced in the previous section, namely $Z_1 = jX_1 = j(+27)$ Ω and $Z_2 = jX_2 = j(-100)$ Ω. Finally, a DC biasing network was designed using large RF-block inductors L_{DC} and a resistor R_{DC} to precisely control the diode biasing current. As can be seen in Fig. 6, the DC paths are then driven to the other side of the substrate by vias, where they can conveniently be connected to the DC voltage references in the antenna environment (see Section V). The PIN diode (Aeroflex Metelics MPN7310A-0805) serves as a low capacitance fast switch, with a negligible transient switching time (orders of nanoseconds) . $Z_{A,a}$ and $Z_{A,b}$ are capacitors of 0.5 pF and 0.8 pF, respectively. The biasing network elements are L_{DC} = 22 nH and $R_{DC} = 910$ Ω.

In order to experimentally validate the reconfigurable load design prior to its insertion in each of the SPA parasitic dipoles, it was fabricated and measured using a thru-reflect-line (TRL) calibration kit, which allows placing the measurement reference planes at the desired locations, as required here. It is then possible to extract the desired impedances Z_1 and Z_2 from the measured S-parameters and microstrip line impedance, as shown in Fig. 5 for each of the diode states. The imaginary parts of the measured impedance Z_1
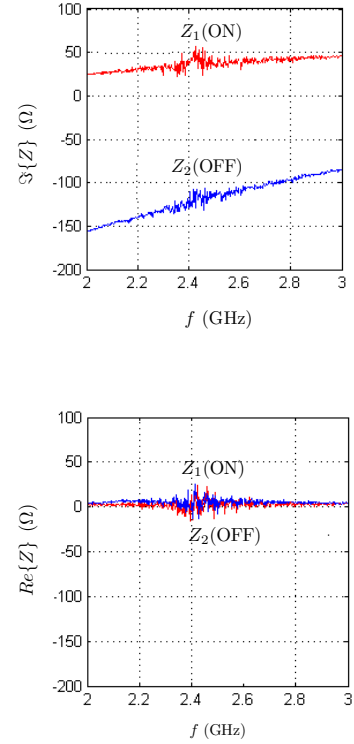

Fig. 5. Measured load impedance in each diode state of the PIN diode, extracted from the S-parameter measurements on a dedicated microstrip TRL calibration kit, from [24]. The OFF and ON diode states correspond to a reversed ($V_{DC} = 0V$) and forward ($I = 9mA$) bias, respectively.

and Z_2 at the design frequency of 2.6 GHz are $+38$ Ω and -108 Ω in the ON and the OFF states, respectively. These values are close to the target reactances of $+27\Omega$ and -100Ω, considering the tolerances of the SMD elements and the impact of the biasing network. The real parts of Z_1 and Z_2 are not exactly zero due the diode and SMD components finite resistances, which were neglected in the design procedure (their measured average values are only $+5$ Ω and $+3$ Ω in the OFF and the ON states, respectively). The target basis functions (at $[X_1 \ X_2]_{opt} = [-100 \ +27] \ \Omega$) and the achieved ones ($[X_1 \ X_2]_{opt} = [-108 \ +38] \ \Omega$) are compared in Fig. 7, showing very good agreement.

V. SIMULATION AND MEASUREMENT RESULTS

The current section presents the measurements of the different SPA parameters and compares them to the corresponding parameters obtained by computer simulations.

A. Antenna Demonstration

A photograph of the fully operational fabricated antenna is shown in Fig. 6. It was observed that a good balanced excitation of the active dipole is simply obtained by connecting the central and the outer conductors of a coaxial connector to each of the dipole arms. The variable load designed and characterized in Section IV.B was introduced in each parasitic
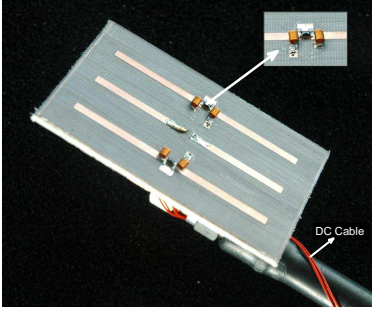
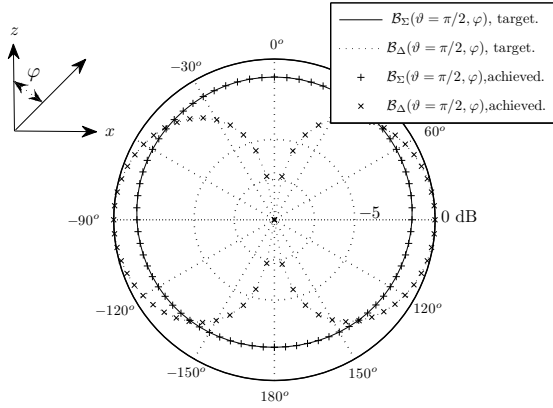Fig. 6. Photograph of the fully operational SPA, optimized for the proposed aerial MIMO approach.

Fig. 7. The magnitude of the H-plane co- polarized basis functions at the target loads of $[+27 \ -100] \ \Omega$ and at the practically achieved loads of $[+38 \ -108] \ \Omega$. The two basis functions resemble the omni and the angular sine functions, which are orthogonal to each other.

Fig. 8. Set-up of the antenna for reconfigurable radiation pattern measurements, with a 9V battery places behind the absorber cone in a direction of the low field intensity.
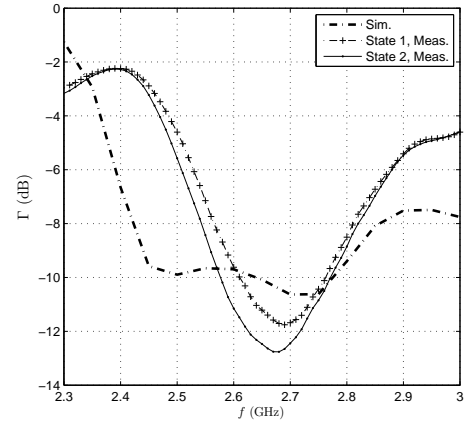

Fig. 9. Return Loss (dB) of the SPA for both loading states i.e. $S := 1$ and $S := 2$.

dipole of the SPA, including the DC biasing network. The DC ground pad of each variable load on the backside of the substrate is connected by a printed line to the coaxial connector outer conductor (which thus serves as a DC ground), whereas each actuation pad (shown as 'V_{DC}' in Fig. 4) is connected by a thin wire to the bias voltages for controlling the states of the diodes. In order to improve the antenna performance and provide pure measured patterns, the DC wires are driven along the coaxial feed, which is oriented toward the minimum radiation of the SPA (i.e. parallel to the dipoles, see Fig. 6). A standard 9V battery is used as a DC source in the radiation pattern measurements. The battery is placed behind a piece of an absorber (located in the direction of minimum radiated power density), as can be seen in Fig. 8. Therefore the antenna states were simply selected by connecting each of the two DC wires to the 0V or 9V references. The impact of the biasing voltages on the antenna performance was investigated, showing similar responses for $-10V$ to $0V$ as the OFF (or 'reverse-biased') state, while $+3V$ to $+10V$ are acceptable for the ON (or 'forward-biased') state.

B. Return Loss

Fig. 9 shows the simulated and measured return loss of the SPA around the design frequency of 2.6 GHz. The graph only shows the response in the operational states of the antenna, namely when it is loaded by the reactance load pairs $[jX_1 \ jX_2]$ and $[jX_2 \ jX_1]$. As explained earlier in Section IV, the return loss is the same for both states due to the SPA symmetry, which is confirmed here by the similarity between the two measured curves in Fig. 9. The SPA was found to have poor matching in the two (unused) states $[jX_1 \ jX_1]$ and $[jX_2 \ jX_2]$), which are not shown here.

The agreement between simulations and the measurements is moderate, since the measured bandwidth is larger than the one obtained by simulation and is not exactly centered around the design frequency of 2.6 GHz. Nevertheless the measurements show good return loss at 2.6 GHz. The -10dB measured bandwidth is 5.6% and 7.1% for a reference of -10 dB, for $S := 1$ and $S := 2$, respectively .

C. Radiation Patterns

Fig. 10 shows the H-plane co- and cross- polarized far fields in the first operational antenna state ($S := 1$). Note that the maximum of the co-polarized beampattern, located at $\varphi = +90°$, corresponds to the direction of the load in the OFF state. The simulated and measured co- and cross-

polarized beampatterns are in good agreement, as shown in Fig 10. Because of the SPA symmetrical structure and the reactance pair antisymmetry, the other antenna beampattern should simply be a mirror image of the first beampattern around the $\varphi = 0° - 180°$ axis, which is well verified by the measured prototype as can be seen in Fig. 11.

D. Experimental Results

The proposed antenna prototype has been successfully used for spatially multiplexing two BPSK datastreams *over the air* at 2.6 GHz. The experiments constitute to the best of the authors' knowledge the first MIMO transmission with a single RF source yet to be proposed. The first train was modulated into a BPSK symbol stream (using a raised-cosine waveform with 0.3 roll-off factor) and up-converted to 2.6 GHz. The high frequency signal was modulated to the central element within a modulation bandwidth of 533 kHz. The second binary train was XORed with the first binary train in the baseband domain and the output baseband control signal was amplified and used for switching the SPA loads. A simple zero-forcing decoding was implemented by the receiver which was equipped with two distant omnidirectional monopole antennas separated from each other by 23cm or 2λ, and both are located several wavelengths from the SPA (the receiver is located in the broadside direction of the SPA, but completely blocked from the transmitter in the sense that no line-of-sight between the transmitter and the receiver exists). The receiver first estimates the receive antennas' responses to the two beampatterns $\mathcal{G}_1(\varphi, \vartheta)$ and $\mathcal{G}_2(\varphi, \vartheta)$ using classical training, then the response to the basis is obtained from (10a,10b). Finally the 2×2 complex channel matrix is inverted and used for equalizing the received signal. A total bit rate of 820 kbps was obtained with arbitrarily low error, thus a spectral efficiency of 1.54 b/s/Hz can be claimed. Although this seems far from the target upperbound of 5 b/s/Hz, it is well justified by the fact of using real signaling with uniform distribution rather than complex signaling with Gaussian distribution. The details of the experiments' setup are detailed in [25].

Fig. 12 shows the received signal constellations after equalization (spatial separation), onto which the transmitted signals (red dots) are also projected, for comparison reasons. Every demodulated signal comprises of two noisy clouds such that $\widehat{\mathbf{x}}_1 = \mathbf{c}_1 \cup \mathbf{c}_2$ and $\widehat{\mathbf{x}}_2 = \mathbf{c}_3 \cup \mathbf{c}_4$. The receive SNR of the ith cloud is calculated as

$$\text{SNR}_i = \frac{\mathbb{E}\left\{\mathbf{c}_i^H \mathbf{c}_i\right\} - \text{Var}\left\{\mathbf{c}_i\right\}}{\text{Var}\left\{\mathbf{c}_i\right\}} \tag{21}$$

where $\mathbb{E}\{.\}$ returns the sample mean of the operand and Var$\{.\}$ returns the sample variance of the operand. The four clouds have almost the same SNR and the mean of the four SNRs is finally considered. The bit SNR referred to as E_b/N_o, is calculated by adding $10\log_{10}(0.5\mathcal{K})$ to the average SNR (in dB), where $\mathcal{K}$ is the number of samples per one symbol whereas the 0.5 factor is due to using real signaling. In this experiment, $\mathcal{K}$ was set to 5 samples per symbol such that each transmission has 410 symbols or equivalently 2048 samples. On the other hand, Fig. 13 shows the bit probability of error
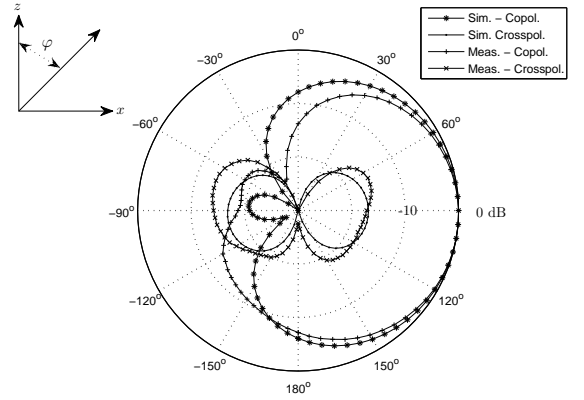

Fig. 10. Simulated and measured co- and cross- polarization components of the beampattern $\mathcal{G}_1(\vartheta, \varphi)$ in the H-plane i.e. $\mathcal{G}_1(\vartheta = \frac{\pi}{2}, \varphi)$, at $f = 2.6$ GHz.
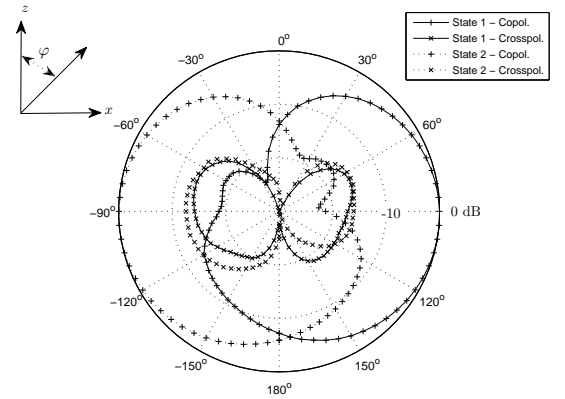

Fig. 11. Measured co- and cross- polarization components of the beam-patterns $\mathcal{G}_1(\vartheta = \frac{\pi}{2}, \varphi)$ and $\mathcal{G}_2(\vartheta = \frac{\pi}{2}, \varphi)$ at $f = 2.6$ GHz. Notice that $\mathcal{G}_1(\vartheta = \frac{\pi}{2}, \varphi) \approx \mathcal{G}_2(\vartheta = \frac{\pi}{2}, -\varphi)$, resulting in a MIPP.

(P_b) versus E_b/N_o obtained by measurements as well as the performance of a 2×2 BPSK-MIMO with a Rayleigh channel of independent and identically distributed coefficients, and zero-forcing decoding[8]. The figure shows that the performance of the beamspace MIMO is comparable to the conventional one, thus validating the importance of such a new approach for realizing single radio compact-sized MIMO transceivers.

VI. CONCLUSION

The paper generalized a previously reported approach for transmitting multiple signals using a single RF source. The idea is to obtain an orthogonal or orthonormal basis out of MIPPs. The paper also provided design steps for an example of a 3-element SPA, capable of forming a MIPP that are mirror images of each other. The SPA was optimized for BPSK signaling by deriving a criterion that maximizes the SPA

[8]Theoretically, P_b of a 2×2 BPSK-MIMO under Rayleigh fading and a zero-forcing receiver is unsurprisingly identical to the performance of 1×1 BPSK-SISO i.e $P_b = 0.5 \left(1 - \sqrt{\frac{E_b/No}{E_b/No+1}}\right)$ [26].
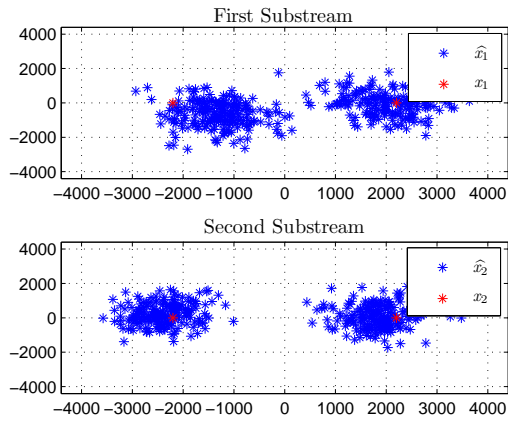
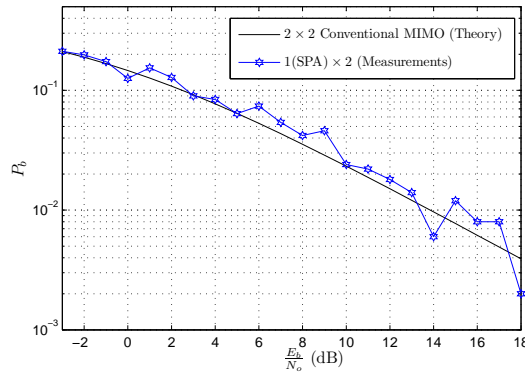Fig. 12. Scatter plot of received signal constellation after equalization.

Fig. 13. Probability of error versus the transmit SNR (per bit).

efficiency and minimizes the power imbalance between the basis functions, simultaneously. A reconfigurable impedance was designed and a fully operational SPA for single radio MIMO transmission was demonstrated for the first time. The measured SPA parameters are in good agreement with the target values, regarding the SPA return loss and the radiation patterns in the different SPA states. Finally, the SPA has been successfully used for multiplexing two BPSK datastreams with a total bit rate of 820 kbps.

ACKNOWLEDGMENT

The authors like to thank Pablo Pardo for fabricating and measuring the variable load circuit, and Pavel Miskovsky for his help in the antenna measurement, both at CTTC.

J. Perruisseau-Carrier thanks the Swiss National Science Foundation (SNSF) for financial support through its professorship program. Finally, the authors express their deepest gratitude to the editor and to the anonymous reviewers for their helpful and constructive comments and suggestions.

APPENDIX

In this part we prove that the cross-correlation of a MIPP in a uniform field is *real*.

Proof: : Assuming a MIPP over the φ angular domain, where φ is the azimuth polar system of coordinates with a reference

axis taken from the MIPP axis of symmetry (the ϑ can be dropped for simplicity). The MIPP can generally be written as $\mathcal{G}_1(\varphi)$ and $\mathcal{G}_2(\varphi) = \mathcal{G}_1(-\varphi)$. The $\mathcal{G}_1(\varphi)$ can be further written as $\mathcal{G}_R(\varphi) + j\mathcal{G}_I(\varphi)$, where $\mathcal{G}_R(\varphi)$ and $\mathcal{G}_I(\varphi)$ are the real and imaginary parts of $\mathcal{G}_1(\varphi)$. The cross-correlation of the MIPP becomes

$$
\begin{aligned}
\varrho_{12} &= \frac{1}{2\pi P} \int_\varphi \mathcal{G}_1(\varphi)\,\mathcal{G}_2^*(\varphi) \cdot d\varphi \\
&= \frac{1}{2\pi P} \int_\varphi \mathcal{G}_1(\varphi)\,\mathcal{G}_1^*(-\varphi) \cdot d\varphi \\
&= \frac{1}{2\pi P} \int_\varphi \left(\mathcal{G}_R(\varphi) + j\mathcal{G}_I(\varphi)\right)\left(\mathcal{G}_R(-\varphi) - j\mathcal{G}_I(-\varphi)\right) \cdot d\varphi \\
&= \frac{1}{2\pi P} \int_\varphi \left(\mathcal{G}_R(\varphi)\mathcal{G}_R(-\varphi) + \mathcal{G}_I(\varphi)\mathcal{G}_I(-\varphi)\right) \cdot d\varphi \\
&\quad + j\frac{1}{2\pi P} \int_\varphi \left(\mathcal{G}_R(-\varphi)\mathcal{G}_I(\varphi) - \mathcal{G}_I(-\varphi)\mathcal{G}_R(\varphi)\right) \cdot d\varphi \\
&= \underbrace{\frac{1}{2\pi P} \int_\varphi \left(\mathcal{G}_R(\varphi)\mathcal{G}_R(-\varphi) + \mathcal{G}_I(\varphi)\mathcal{G}_I(-\varphi)\right) \cdot d\varphi}_{\text{real}}
\end{aligned}
$$

■

REFERENCES

[1] J. H. Winters,"On the capacity of radio communication systems with diversity in a Rayleigh fading environment," *IEEE J. Select Areas Commun.*, vol. SAC-5, pp. 871878, June 1987.
[2] G. J. Foschini and M. J. Gans,"Limits of wireless communication in a fading environment when using multiple antennas," *Wireless Personal Communications,* . 6, pp. 311-335, 1998.
[3] Overview of 3GPP Release 8 V0.0.3, November 2008, available online at http://www.3gpp.org/Release-8.
[4] J. Kotecha, "LTE:MIMO Techniques in 3GPP-LTE," *Freescale Semiconductor*, June 2008.
[5] M. Okoniewski, S. V. Hum, A. Sutinjo, and G. G. Messier, "A spacetime coding scheme utilizing phase shifting antennas at RF frequencies," *IEEE Antennas and Wireless Propagation Letters*, vol. 4, Page(s): 369 - 372, 2005.
[6] J. Yuan and B. Vucetic," *Space-Time Coding*, John Wiley & Sons Ltd, 2003.
[7] A. Grau, J. Romeu, M. Lee, S. Blanch, L. Jofre and F. De Flaviis, "A Dual-Linearly-Polarized MEMS-Reconfigurable Antenna for Narrowband MIMO Communication Systems," *IEEE Transactions on Antennas and Propagation*, vol. 58, no. 1, January 2010.
[8] M. Wennstrom and T. Savantesson, "An antenna solution for MIMO channels: the switched parasitic antenna," *IEEE International Symposium on Personal, Indoor and Mobile Radio Communications, 2001 12th*, vol.1, pp 159-163, September 2001.
[9] R. Vaughan, "Switched Parasitic Elements for Antenna Diversity," *IEEE Transactions on Antennas and Propagations*, vol.47, no.2, Feb-1999.
[10] T. Sawaya, K. Iigusa, M. Taromaru, T. Ohira, "Reactance diversity: proof-of-concept experiments in an indoor multipath-fading environment with a 5-GHz prototype planar ESPAR antenna," *Consumer Communications and Networking Conference*, 5-8 Jan. 2004, pp. 678-680.
[11] M. Yamamoto, M. Taromaru, H. Sadamichi and A. Shimizu, "Performance of Angle Switch Diversity Using ESPAR Antenna for Mobile Reception of Terrestrial Digital TV," *Vehicular Technology Conference*, Fall-2006.
[12] C. Sun, A. Hirata, T. Ohira, and N. C. Karmakar,"Fast Beamforming of Electronically Steerable Parasitic Array Radiator Antennas: Theory and Experiment," *IEEE Transactions on Antennas and Propagation*, vol. 52, no. 7, July 2004.
[13] A. Kalis, A. G. Kanatas and C. B. Papadias, "A novel approach to MIMO transmission using a single RF front end," IEEE Journal on Selected Areas in Communications, vol. 26, No. 6, Aug. 2008.
[14] O. N. Alrabadi C. B. Papadias, A. Kalis and R. Prasad, "A Universal Encoding Scheme for MIMO Transmission Using a Single Active Element for PSK Modulation Schemes," *IEEE Transactions on Wireless Communications*, pages: 5133 - 5142, vol. 8, No. 10, October 2009.

[15] A. S. Y. Poon, R. W. Brodersen, and D. N. C. Tse, "Degrees of freedom in multiple-antenna channels: a signal space approach," *IEEE Trans. on Information Theory*, vol. 51, no. 2, pp. 523-536, Feb. 2005.

[16] M. L. Morris and M. A. Jensen,, "Network Model for MIMO Systems With Coupled Antennas and Noisy Amplifiers,"*IEEE Transactions on Antennas and Propagation*, vol.53, no.1, Jan. 2005.

[17] C. Waldschmidt, S. Schulteis, and W. Wiesbeck, "Complete RF System Model for Analysis of Compact MIMO Arrays," *IEEE Trans. on Veh. Tech.*, vol. 53, no. 3, May 2004.

[18] D. M. Pozar, "The active element pattern", *IEEE Trans. on Antennas and Propagation*, vol. 42, no. 8, Aug 1994.

[19] L. Petit, L. Dussopt and J. Laheurte, "MEMS-Switched Parasitic-Antenna Array for Radiation Pattern Diversity," *IEEE Transactions on Antennas and Propagation*, vol. 54, no. 9, Sep 2006.

[20] D. S. Shiu, G. J. Foschini, M. J. Gans and J. M. Kahn, "Fading correlation and its effect on the capacity of multielement antenna systems," *IEEE Trans. Commun.*, vol. 48, no. 3, pp. 502-513, Mar. 2000.

[21] Y. Fei, Y. Fan, B. K. Lau, and J. S. Thompson, "Optimal Single-Port Matching Impedance for Capacity Maximization in Compact MIMO Arrays," *IEEE Trans. Antennas and Propagation*, vol. 56, no. 11, Nov. 2008.

[22] A. Paulraj, R. Nabar and D. Gore, "Introduction to Space-Time Wireless Communications," *Cambridge, U.K.: Cambridge Univ. Press*, 2003.

[23] R. A. Horn, "Matrix analysis," *Cambridge university press*, 1996.

[24] J. Perruisseau-Carrier, O. N. Alrabadi, and A. Kalis,"Implementation of a Reconfigurable Parasitic Antenna for Beam-Space BPSK Transmissions," *2010 European Microwave Conference (EuMA)*, Paris, France, September 2010, Page(s): 644 - 647.

[25] O. N. Alrabadi et al, "Spatial Multiplexing with a Single Radio: Proof-of-Concept Experiments in an Indoor Environment with a 2.6 GHz Prototype," *IEEE Communications Letters*, pp. 178-180, vol. 15, no. 2, 17 Dec. 2010.

[26] D. Tse and P. Viswanath, "Fundamentals of Wireless Communication," *Cambridge University Press*, 2005.